Theoretical and Experimental Study of Relaxations in Al_3Ti and Al_3Zr Ordered Phases

C. Amador,[1,*] J. J. Hoyt,[1,†] B. C. Chakoumakos,[2] and D. de Fontaine[1]

[1]*Department of Materials Science, University of California, Berkeley, California 94720 and Lawrence Berkeley Laboratory, Materials Science Division, Berkeley, California 94720*

[2]*Solid State Division, Oak Ridge National Laboratory, Oak Ridge, Tennessee 37831*

(Received 22 November 1994)

The aim of the present investigation was to elucidate the role of structural relaxations in determining the relative stability of $L1_2$, $D0_{22}$, and $D0_{23}$ structures in Al_3Ti and Al_3Zr. This task was accomplished by a unique combination of total-energy electronic structure calculations and (for Al_3Zr) high resolution neutron diffraction with Reitveld refinement. Calculated and measured atomic displacements are in excellent agreement. Local relaxation is found to be responsible for the stability of the $D0_{23}$ structure in Al_3Zr, in agreement with experimental evidence.

PACS numbers: 81.30.Bx, 61.12.Gz, 61.66.Dk, 71.20.Cf

Titanium and zirconium trialuminides are promising structural materials because of their high melting points, low densities, and oxidation resistance. However, their applicability has been hindered by their poor ductility. The ground state structures of Al_3M alloys (where M is the IVB transition metal element, Ti, Zr, or Hf) are $D0_{22}$ or $D0_{23}$, which have tetragonal symmetry and therefore not enough equivalent slip systems to operate in polycrystalline materials. Hence, a large number of studies, both experimental and theoretical, have been undertaken in recent years in attempts to stabilize the cubic $L1_2$ structure in these and related alloys, some of the literature on the subject having been reviewed by Asta *et al.* [1].

Of the $L1_2$, $D0_{22}$, and $D0_{23}$ crystal structures, the latter two may be considered as superstructures of the simple cubic $L1_2$ cell. The $D0_{22}$ unit cell consists of two $L1_2$ cubes stacked along, say, the z direction, with a $[\frac{1}{2}\ \frac{1}{2}\ 0]$ antiphase shift between the cubes; the $D0_{23}$ structure consists of a stacking of four $L1_2$ cubes with the same antiphase shifts every two cubes. Hence, in the axial next nearest neighbor Ising (ANNNI) model notation [2] as applied to antiphase structures [3] the period of antiphase boundaries is $\langle\infty\rangle$ for $L1_2$, $\langle 1\rangle$ for $D0_{22}$, and $\langle 2\rangle$ for $D0_{23}$.

From $L1_2$ to $D0_{22}$ to $D0_{23}$, symmetry elements are progressively lost, so that relaxation degrees of freedom increase correspondingly. In $L1_2$ energy may be optimized with respect to atomic volume (or lattice parameter a) only, in $D0_{22}$ energy optimization may be performed additionally with respect to c/a ratio, and in $D0_{23}$ additionally with respect to the two types of displacements δ_1 and δ_2 indicated in Fig. 1, since the z coordinates of these atomic coordinates are not fixed by symmetry (Wyckoff positions $4e$ for $D0_{23}$ space group $I4/mmm$). In recent years the importance of including atomic displacements in total energy calculations of ordered compounds has been recognized [4]. In previous studies [1,5,6] it was demonstrated that the tetragonal phases of group IVB trialuminides could only be stabilized with respect to the cubic $L1_2$ by allowing for c/a relaxation. Carlsson and Meschter [5] used c/a ratios deduced from experiment in their calculations and attributed the failure to predict the correct $D0_{23}$ ground state for Al_3Zr to approximations made in the calculations. The true cause of the discrepancy, as will now be shown, is the neglect of the additional internal degrees of freedom (δ_1 and δ_2) of the $D0_{23}$ structure. The present study is the first that optimizes the energy calculations with respect to all possible structural degrees of freedom; moreover, it will be shown that the calculated δ_1 and δ_2 values for Al_3Zr are in excellent agreement with neutron diffraction determination of these displacements, performed concurrently.

Cohesive energies were calculated at absolute zero temperature for fcc Al, Ti, and Zr, and for the $L1_2$, $D0_{22}$, and

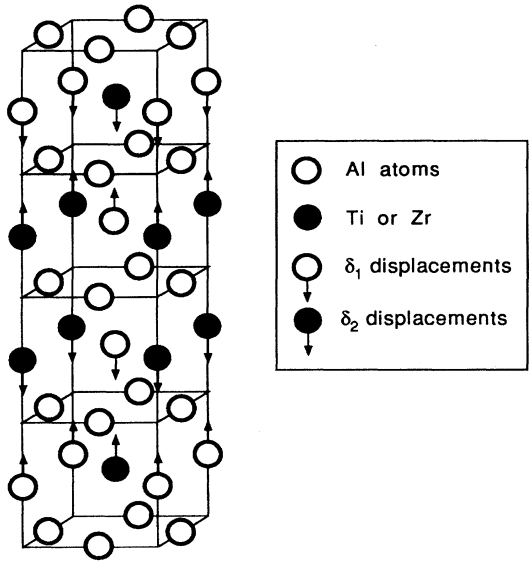

FIG. 1. Unit cell of the $D0_{23}$ structure. Al and Ti or Zr atoms can move off their ideal positions by two crystallographically distinct displacements δ_1 and δ_2.

0031-9007/95/74(24)/4955(4)$06.00

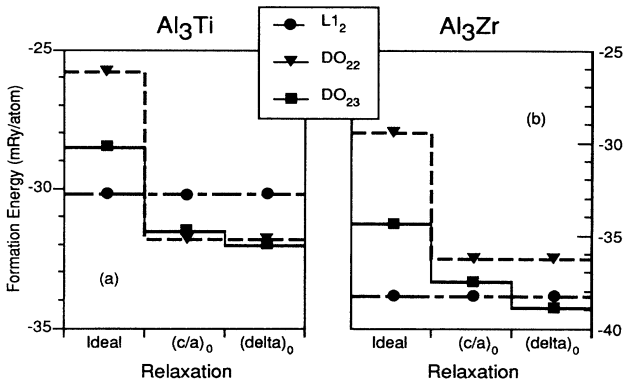

FIG. 2. Formation energies of the three different structures in the three stages of relaxation (see text). (a) Al_3Ti, (b) Al_3Zr.

$D0_{23}$ structures of Al_3Ti and Al_3Zr, optimized with respect to all possible structural degrees of freedom. No vibrational entropy contributions were included. Computations were carried out by means of the full-potential linear muffin-tin orbital (FP-LMTO) method in the version developed by Methfessel and Van Schilfgaarde [7]. For the three structures, $L1_2$, $D0_{22}$, and $D0_{23}$, whose unit cells contain 4, 4, and 8 atoms, respectively, the Brillouin zone was divided into a mesh of 13^3 points; thus 86, 196, and 196 k points were used for these structures. Errors associated with this finite sampling are estimated to be about 0.5 mRy/atom. The basis set consisted of 22 orbitals per atom, corresponding to three different kinetic energies (s-, p-, and d-like for the first two energies, s and p for the third). In the case of Zr, the $4s$ and $4p$ states are rather low so that semicore states were treated in a second energy panel where an extra 22 orbitals were used. The expansion of two-center products in the interstitial region was done in terms of Hankel functions of two different kinetic energies truncated for $l_{\max} > 6$. The internal precision of the calculations for the basis selected was expected to be better than 0.2 mRy/atom.

Formation energies (energy of the compound minus the concentration-weighted average of the elements in the fcc structure) are shown in Fig. 2 for Al_3Ti and Al_3Zr, for the three competing structures, and for three stages of the relaxation process: volume, c/a ratio, and cell-internal displacements; in all, 12 energies are represented. In the "ideal" case, all atoms occupy the lattice sites of an fcc lattice with lattice parameter optimized for the compound in question. The notation $(c/a)_0$ denotes energies calculated after c/a relaxation (of course $L1_2$ is unaffected) and $(\text{delta})_0$ denotes $D0_{23}$ energies optimized for δ_1 and δ_2 relaxations. Values of lattice parameters and displacements δ_1 and δ_2 are reported in Table I for Al_3Ti and in Table II for Al_3Zr. For the lattice parameter in the z direction, normalized values are given: $c' = c/2$ for $D0_{22}$ and $c' = c/4$ for $D0_{23}$.

TABLE I. Lattice parameter and atomic displacements (δ_1 and δ_2) for Al_3Ti. Normalized lattice parameter $c' = c/2$ for $D0_{22}$ and $c' = c/4$ for $D0_{23}$. Full-potential LMTO values are compared with experimental values determined by Srinivasan, Desch, and Schwarz (SDS) [8] and by van Loo and Rieck (vLR) [9].

Al_3Ti structure	Lattice parameter	FP-LMTO	SDS	vLR
$L1_2$	a (Å)	3.97	3.967	...
$D0_{22}$	a (Å)	3.76	3.851	3.849
	c' (Å)	4.25	4.306	4.305
	c'/a	1.13	1.118	1.118
$D0_{23}$	a (Å)	3.81	3.890	3.875
	c' (Å)	4.11	4.206	4.229
	c'/a	1.08	1.0811	1.091
	δ_1	−0.006	...	...
	δ_2	−0.026	...	...

In the ideal case, $L1_2$ (circles, dot-dashed lines) has the lowest formation energy, followed by $D0_{22}$ (squares, unbroken lines), then by $D0_{23}$ (triangles, dashed line) for both compounds. At the $(c/a)_0$ stage, the order remains the same for Al_3Zr but is completely reversed for Al_3Ti. After the $(\text{delta})_0$ relaxation stage, $D0_{23}$ becomes the favored structure for both alloys, although the difference between $D0_{22}$ and $D0_{23}$ for Al_3Ti is extremely small, 0.2 mRy/atom. That difference is of the order of the accuracy of the full-potential LMTO total-energy calculations. Although the relative error in comparing two similar structures for the same intermetallic compound may be much less, the computed energy difference between $D0_{22}$ and $D0_{23}$ is still too small to make definitive conclusions as to the true ground state of Al_3Ti. However, a very small difference in calculated energies suggests that long-period superstructures are likely to form in Al_3Ti and, in fact, there is experimental evidence for the existence of such structures [9,10]. Our calculated energy differences agree with those obtained experimentally, where available (see Ref. [1] for a review of results for Al_3Ti). From the foregoing, it is seen that the internal atomic displacements

TABLE II. Lattice parameter and atomic displacements (δ_1 and δ_2) for Al_3Zr in the $D0_{23}$. Normalized lattice parameter $c' = c/4$. Full-potential LMTO values are compared with those obtained by neutron diffraction at 12 K and at room temperature, and to those obtained by Srinivasan, Desch, and Schwarz (SDS) [7] by x-ray diffraction.

Al_3Zr lattice parameter	FP-LMTO	12 K	Room temperature	SDS
a (Å)	3.91	4.0012	4.0080	4.009
c' (Å)	4.26	4.3111	4.3206	4.320
c'/a	1.09	1.0775	1.0780	1.078
δ_1	+0.003	+0.0004	0.0000	...
δ_2	−0.026	−0.0272	−0.0253	...

δ_1 and δ_2 are essential for stabilizing the correct $D0_{23}$ ground state for Al_3Zr. Since there appear to be no previous determinations of these δ displacements, either experimental or theoretical, it was decided to perform a neutron diffraction analysis of a powder sample of Al_3Zr, the $D0_{23}$ structure of Al_3Ti not being accessible.

Alloys were prepared from >99.999% Al and >99.99% Zr by arc melting in an Ar atmosphere. Metallography and x-ray powder diffraction revealed the presence of a small amount of the Al_2Zr phase located at grain boundaries, indicating a slight loss of Al during the sample preparation. The very small volume fraction of the impurity phase (<1%) had no effect on the structural parameters measured. About 3 cm^3 of material was ground to a final particle size of approximately 0.1–0.5 mm. The powdered sample was placed in a vanadium cylinder under a He atmosphere. Neutron diffraction data were taken at room temperature and, since the electronic structure code is a ground state computation, at a temperature of 12 K.

Neutron scattering experiments were performed on the high resolution powder diffractometer (beam line HB-4) at the High Flux Isotope Reactor (HFIR) located at the Oak Ridge National Laboratory. An incident energy of $\lambda = 1.4177$ Å, corresponding to the (115) reflection from a Ge monochromator, was employed. The 2θ scan range was 11° to 135° at a step size of 0.05°.

A 20 parameter Reitveld refinement of 131 Bragg peaks for both 12 K and room temperature scans ($\chi^2 = 2.171$, $Rwp = 0.0761$) returned the data reported in Table II. Another experimental determination [8] of a and c' is also shown for comparison. Given the local density approximation's (LDA) well-known tendency to underestimate lattice parameters, agreement between measured and calculated values is very good. The lattice parameter ratios are in excellent agreement. More importantly for the present analysis, neutron diffraction and FP-LMTO values of δ_1 and δ_2 agree closely, in sign and magnitude. These displacements thus create a slight "rumpling" of the lattice plane on which they operate.

Since the three competing structures under consideration here differ by their antiphase boundary sequencing, it is convenient to parametrize the corresponding formation energies by means of effective planar (or "axial") interactions J_1 and J_2, as was done previously for the case of periodic antiphase boundary structures [3]. In this model of an Al_3M alloy, J_1 is an effective pair interaction (EPI) coupling sites on the "mixed" Al-M planes separated (nominally) by distance a along the z direction, and interaction J_2 couples sites separated by $2a$, also along this axial direction. The Ising model representation of the formation energy is then, after suitable normalization,

$$\Delta E = E_0 + J_1 \sum_p \sigma_p \sigma_{p+1} + J_2 \sum_p \sigma_p \sigma_{p+2}, \quad (1)$$

where $\sigma_p = +1$ (-1) is an Al (M) atom which occupies site p, p denoting the position of a mixed lattice plane. E_0 contains all other interactions including those pertaining to the "unmixed" pure Al planes. We then have from Eq. (1)

$$\begin{aligned} E_{L1_2} &= E_0 + 4J_1 + 4J_2, \\ E_{D0_{22}} &= E_0 - 4J_1 + 4J_2, \\ E_{D0_{23}} &= E_0 - 4J_2. \end{aligned} \quad (2)$$

The formation energies ΔE having been calculated (see Fig. 1), system (2) can be inverted to yield the EPI J_1 and J_2 (also E_0) for each alloy at each stage of the relaxation process. Results are shown diagrammatically in Fig. 3 where filled circles, shaded circles, and filled squares designate EPI's for ideal, c/a-relaxed, and δ-relaxed structures, respectively, letters T and Z denoting values pertaining to Al_3Ti and Al_3Zr, respectively. The three heavy lines intersecting at the origin delimit regions of stability of $L1_2$, $D0_{22}$, and $D0_{23}$ structures. Negative first-neighbor (J_1) interactions favor $L1_2$ (or $\langle\infty\rangle$ in ANNNI model notation), whereas positive J_1 interactions favor $D0_{22}$ (or $\langle 1\rangle$). This tendency can be understood as follows: If J_2 is small in magnitude with respect to J_1, the antiphase boundary (APB) energy is proportional to J_1; with $J_1 < 0$ these APB's raise the energy of the system, with $J_1 > 0$, the APB's lower the energy and tend towards maximum density. When the second-neighbor effective interaction J_2 is positive, frustration occurs: second neighbors would prefer to be unlike ($\sigma_p \sigma_{p+2} = -1$), thereby prohibiting *both* intermediate first-neighbor interactions from being satisfied, whether J_1 be positive or negative. The long-period APB structure $D0_{23}$ is just the simplest way of dealing with the frustrated situation. An infinity of increasingly complex long-period structures are

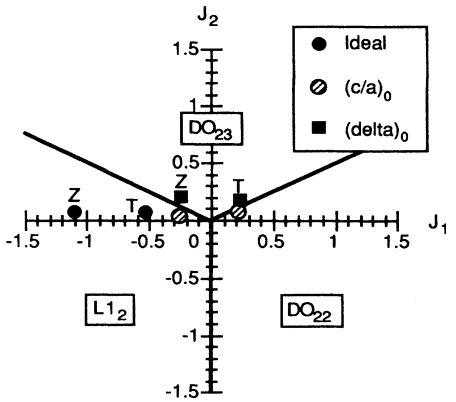

FIG. 3. Ground state phase diagram for the ANNNI model in the space of the interaction parameters J_1 and J_2. Stable structures for each region are indicated. The points correspond to the parameters obtained from the full-potential calculated formation energies for Al_3Ti (T) and Al_3Zr (Z). Three sets of parameters are plotted; full circles correspond to the ideal structures, shaded circles to the c/a-relaxed structures, and squares to the fully relaxed ("δ") structures. Units are mRy/atom.

also possible, but these can only be stabilized by entropy effects or by the presence of longer range EPI's [2,3,11].

In agreement with the results of Fig. 2, it is seen that the representative points of the alloys ("T" or "Z") in the J_1-J_2 ground state map (Fig. 3) evolve from the $L1_2$ to the $D0_{23}$ region as relaxation is allowed to occur. The intermediate states (shaded circles) differ: $L1_2$ in the case of Al_3Zr, $D0_{22}$ in the case of Al_3Ti. Also, $D0_{22}$ is the second most favored structure at equilibrium for Al_3Ti, while it is $L1_2$ for Al_3Zr. The latter result may explain why Al_3Zr precipitates of $L1_2$ structure are observed in Al-rich Al-Zr alloys [12]. Note that c/a relaxation alone causes the representative alloy point (J_1,J_2) to evolve almost horizontally (parallel to the J_1 axis), while the final δ relaxation causes a vertical evolution of the point: shaded circle to filled square. It can indeed be shown from Eq. (2) that δ relaxation leaves the J_1 value invariant. Clearly, the slight rumpling of the pertinent (001) lattice planes ($\delta_1 \neq \delta_2$) causes the effective J_2 to increase, thereby stabilizing the $D0_{23}$ structure, as mentioned above.

In conclusion, we have performed the first calculations of internal atomic relaxations in Al_3Ti and Al_3Zr and also the first experimental determinations of these displacements in the case of Al_3Zr. For this alloy, agreement between measured and calculated displacements was excellent, thereby lending support to the statement that it is this particular internal relaxation which stabilizes the $D0_{23}$ structure. For Al_3Ti, and contrary to expectations, the $D0_{23}$ structure was calculated to be the stable ground state at low temperature, but by a very small margin. These two alloys do differ in their relaxation behaviors, as shown by a phenomenological ANNNI model description in terms of effective planar interactions.

One of the authors (C. A.) is indebted to Dr. Mark Van Schilfgaarde for providing him with the latest version of the full-potential LMTO code and for many helpful comments. J. J. H. was supported by the National Science Foundation under Contract No. DMR 9301220. The Oak Ridge National Laboratory is operated by Martin Marietta Energy Systems, Inc. for the U.S. Department of Energy under Contract No. DE-AC05-84OR21400. The work of D. d. F. was supported by the Director, Office of Energy Research, Office of Basic Energy Sciences, Materials Sciences Division of the U.S. Department of Energy under Contract No. DE-AC03-76SF00098. Computational services from the Dirección General de Servicios de Cómputo Académico–UNAM–México are gratefully acknowledged.

*On sabbatical leave from Falcultad de Química, Universidad Nacional Autónoma de México.

†On sabbatical leave from Washington State University, St. Louis, MO 63130.

[1] M. Asta, D. de Fontaine, M. van Schilfgaarde, M. Sluiter, and M. Methfessel, Phys. Rev. B **46**, 5055 (1992); M. Asta, D. de Fontaine, and M. van Schilfgaarde, J. Mater. Res. **8**, 2554 (1993).

[2] M. E. Fisher and W. Selke, Phys. Rev. Lett. **44**, 1502 (1980).

[3] D. de Fontaine and J. Kulik, Acta Metall. **33**, 145 (1985).

[4] Z. W. Lu, S.-H. Wei, A. Zunger, S. Frota-Pessoa, and L. G. Ferreira, Phys. Rev. B **44**, 512 (1991); A. Zunger, in *Statics and Dynamics of Alloy Phase Transformations,* edited by P. E. A. Turchi and A. Gonis (Plenum Press, New York, 1994).

[5] A. E. Carlsson and P. J. Meschter, J. Mater. Res. **4**, 1060 (1989).

[6] D. M. Nicholson, G. M. Stocks, W. M. Temmerman, P. Sterne, and D. G. Pettifor, Mater. Res. Soc. Symp. Proc. **133**, 19 (1989).

[7] M. Methfessel, Phys. Rev. B **38**, 1537 (1988); M. Methfessel, C. O. Rodríguez, and O. K. Andersen, Phys. Rev. B **40**, 2009 (1989); M. Methfessel and M. van Schilfgaarde, Phys. Rev. B **48**, 4937 (1993).

[8] S. Srinivasan, P. B. Desch, and R. B. Schwarz, Scripta Metall. Mater. **25**, 2516 (1991).

[9] F. J. J. van Loo and G. D. Rieck, Acta Metall. **21**, 61 (1973).

[10] A. Loiseau and C. Vannuffel, Phys. Status Solidi A **107**, 655 (1988).

[11] D. de Fontaine, G. Ceder, and M. Asta, Nature (London) **343**, 544 (1990).

[12] E. Nes, Acta Metall. **20**, 499 (1972).